Open access • Journal Article • DOI:10.1103/PHYSREVB.98.094415

Magnetism and exchange-bias effect at the MnN/Fe interface — Source link

Eszter Simon, Rocio Yanes, Sergii Khmelevskyi, Krisztián Palotás ...+4 more authors

Institutions: Budapest University of Technology and Economics, University of Salamanca, Vienna University of Technology, Slovak Academy of Sciences ...+2 more institutions

Published on: 13 Sep 2018 - Physical Review B (American Physical Society)

Topics: Antiferromagnetism, Exchange bias, Spin model, Ferromagnetism and Magnetism

Magnetism and exchange-bias effect at the MnN/Fe interface

E. Simon,[1,*] R. Yanes,[2] S. Khmelevskyi,[3] K. Palotás,[1,4,5] L. Szunyogh,[1,6] and U. Nowak[7]

[1]*Department of Theoretical Physics, Budapest University of Technology and Economics, Budafoki út 8, H-1111 Budapest, Hungary*

[2]*Department of Applied Physics, University of Salamanca, E-37008 Salamanca, Spain*

[3]*Center for Computational Materials Science, Institute for Applied Physics, Vienna University of Technology, Wiedner Hauptstrasse 8, A-1060 Vienna, Austria*

[4]*Department of Complex Physical Systems, Institute of Physics, Slovak Academy of Sciences, SK-84511 Bratislava, Slovakia*

[5]*MTA-SZTE Reaction Kinetics and Surface Chemistry Research Group, University of Szeged, H-6720 Szeged, Hungary*

[6]*MTA-BME Condensed Matter Research Group, Budapest University of Technology and Economics, Budafoki út 8, H-1111 Budapest, Hungary*

[7]*Department of Physics, University of Konstanz, D-78464 Konstanz, Germany*

(Received 10 May 2018; revised manuscript received 23 July 2018; published 13 September 2018)

Based on *ab initio* calculations and spin dynamics simulations, we perform a detailed study on the magnetic properties of bulk MnN and the MnN/Fe interface. We determine the spin model parameters for the θ-phase of bulk MnN, and we find that the competition between the nearest and the next-nearest-neighbor interactions leads to antiferromagnetic ordering of the Mn spins, in agreement with previous theoretical and experimental results. At the MnN/Fe interface, a sizable Dzyaloshinskii-Moriya interaction appears leading to a stable exchange-bias effect. We study the dependences of the exchange-bias effect on the thicknesses of the ferromagnetic and the antiferromagnetic layers, and we compare them to experimentally obtained results [Meinert *et al.*, Phys. Rev. B **92**, 144408 (2015)].

DOI: 10.1103/PhysRevB.98.094415

I. INTRODUCTION

The exchange-bias (EB) effect, which is related to the shift of the hysteresis loop of a ferromagnet relative to the zero-field position [1], is employed for a variety of technological applications in spintronic devices. A typical example is a spin valve composed of two ferromagnetic layers, namely a free sensing layer and a fixed (pinned) reference layer, separated by a nonmagnetic layer. While the free ferromagnet (FM) follows the external magnetic field, the second ferromagnetic layer is pinned via the EB effect, which is caused by the interfacial interaction with an antiferromagnet (AF). The microscopic origin of the EB has been discussed for a long time, and it seems that there is no single origin of EB but rather a variety of effects that play a role, such as the roughness of the FM-AF interfaces [2,3], domains in the AF pinned by defects [4–6], uncompensated interfacial spins [7], anisotropic exchange interactions across the interface [8], and a granular structure of the AF [9]. While these models rest on statistical arguments, where different types of disorder break the balance between magnetic moments in the two sublattices of the AF, recently, based on symmetry properties, Dzyaloshinskii-Moriya (DM) interactions have been proposed as a possible mechanism responsible for EB in perfectly compensated systems [10–12]. Moreover, the EB is related to the coupling between the FM and the AF, and the stability of this coupling is provided by the AF. For this reason, the magnetic properties of the AF are important in the formation of the EB effect.

Commonly used antiferromagnets in devices with EB functionality are IrMn and PtMn [13–15], both causing large and stable EB effects. FeMn and NiMn are known alternatives that also produce an EB effect, but the ratios of the exchange bias to the coercive fields are less ideal for technological applications [14]. Because of this technological relevance, the quest for new antiferromagnetic materials avoiding scarce elements is an important topic of modern material research [16], and, in a recent work of Meinert *et al.* [17], it was shown that in the case of polycrystalline MnN/CoFe interfaces a strong exchange-bias effect exists. Although this material combination displays a nonmonotonic dependence of the EB field on both the AF and FM thicknesses, this work indicates the possibility to use MnN as antiferromagnetic material in future magnetic devices.

While different chemical compositions of Mn and N are known in the literature [18], in the following we focus on MnN in a slightly tetragonally distorted rocksalt phase at room temperature, which corresponds to the θ phase. The magnetic order of bulk MnN was investigated by neutron powder diffraction measurements [19,20] and by theoretical calculations [18,21]. These studies showed that the magnetic order is collinear AF-I type, where the magnetic moments of the Mn are coupled ferromagnetically within the planes perpendicular to the c axis and antiferromagnetically between such planes along the c axis.

Motivated by the experimental study in Ref. [17], we investigate the magnetic properties of the θ-phase of bulk MnN and the MnN/Fe interface at zero and finite temperatures

*esimon@phy.bme.hu

using a multiscale model: we first calculate spin-model parameters *ab initio* and subsequently perform atomistic spin-dynamic simulations. We find that the magnetic ground state of MnN is AF-I type, in agreement with previous theoretical investigations [18,21], and the calculated Néel temperature agrees well with the experimental value. In the case of the MnN/Fe interface, the spin-model parameters are derived after determining the optimal interface geometry. Interestingly, a sizable Dzyaloshinskii-Moriya interaction appears that gives rise to large EB. Studying the thickness dependence of the EB effect, we find that a rather large AFM thickness is needed to stabilize the EB, in agreement with recent experiments [17].

II. MODEL AND NUMERICAL APPROACH

The self-consistent calculations for both the MnN bulk and the MnN/Fe interface system are performed by using of the fully relativistic screened Korringa-Kohn-Rostoker method [22,23]. The electronic structure was determined in the paramagnetic state in terms of the scalar-relativistic disordered local moment (DLM) approach [24], while the spin-cluster expansion technique as combined with the relativistic DLM technique [25] was employed to derive the exchange interactions. The magnetic properties are well described by the following extended classical spin model:

$$H = -\frac{1}{2}\sum_{i\neq j}\vec{s}_i J_{ij}\vec{s}_j - \frac{1}{2}\sum_{i\neq j} B_{ij}(\vec{s}_i\cdot\vec{s}_j)^2 + \sum_i K_i(\vec{s}_i\cdot\vec{e}_i)^2 - \sum_i \mu_i(\vec{s}_i\cdot\vec{H}_a), \quad (1)$$

where $\vec{s}_i$ is the unit vector along the direction of the spin moment of atom i. In the Hamiltonian (1), the first term corresponds to a generalized Heisenberg model where J_{ij} are the tensorial exchange interactions. The second term describes the isotropic biquadratic interaction between spins i, j with the coupling constants B_{ij}. In the case of uniaxial systems, K_i stands for the on-site anisotropy energy of the spin moment of atom i, and $\vec{e}_i$ is the direction of the corresponding easy or hard axis. The last term in the Hamiltonian is the Zeeman energy, with $\vec{H}_a$ the applied field.

The matrix of exchange interactions J_{ij} can further be decomposed into three terms: $J_{ij} = J_{ij}^{\text{iso}}\mathcal{I} + J_{ij}^{S} + J_{ij}^{A}$ [26], with $J_{ij}^{\text{iso}} = \frac{1}{3}\text{Tr}[J_{ij}]$ the isotropic exchange interaction; $J_{ij}^{S} = \frac{1}{2}(J_{ij} + J_{ij}^{T}) - J_{ij}^{\text{iso}}\mathcal{I}$ the traceless symmetric part; and $J_{ij}^{A} = \frac{1}{2}(J_{ij} - J_{ij}^{T})$ the antisymmetric part of the exchange tensor. The latter is clearly related to the DM interaction, $\vec{s}_i J_{ij}^{A}\vec{s}_j = \vec{D}_{ij}\cdot(\vec{s}_i\times\vec{s}_j)$, with $\vec{D}_{ij}$ the DM vector. The DM interaction arises due to the spin-orbit coupling and favors a perpendicular alignment of the spins $\vec{s}_i$ and $\vec{s}_j$ [27,28]. In the case of tetragonal symmetry, the diagonal terms of the traceless symmetric part induce an energy difference between the uniformly magnetized states along the out-of-plane (z) and in-plane (x) directions,

$$\Delta J = \sum_i \Delta J_i, \quad (2)$$

with the site-resolved contributions,

$$\Delta J_i = \frac{1}{2}\sum_{j(\neq i)}\left(J_{ij}^{zz} - J_{ij}^{xx}\right). \quad (3)$$

ΔJ is referred to as the two-site anisotropy, and the total magnetic anisotropy energy of the system can be expressed as a sum of the on-site and two-site contributions.

To study the magnetic properties in the ground state of the system, as well as at elevated temperatures, we solve the stochastic Landau-Lifshitz-Gilbert (SLLG) equation on a discrete lattice,

$$\frac{\partial\vec{s}_i}{\partial t} = -\frac{\gamma}{(1+\alpha^2)\mu_s}\vec{s}_i\times(\vec{H}_i + \alpha\,\vec{s}_i\times\vec{H}_i), \quad (4)$$

by means of Langevin dynamics, using a Heun algorithm [29,30] and considering the additional spin-transfer torque. The SLLG equation includes the gyromagnetic ratio γ, a phenomenological damping parameter α, and the effective field,

$$\vec{H}_i = \vec{\zeta}_i(t) - \frac{\partial H}{\partial\vec{s}_i} = \vec{\zeta}_i(t) - 2K_i(\vec{s}_i\cdot\vec{e}_i)\vec{e}_i + \sum_{j(\neq i)} J_{ij}\vec{s}_j + 2\sum_{j(\neq i)} B_{ij}(\vec{s}_i\cdot\vec{s}_j)\vec{s}_j + \mu_i\vec{H}_a, \quad (5)$$

which considers the influence of a temperature T by adding a stochastic noise term $\vec{\zeta}_i(t)$, obeying the properties of white noise [31],

$$\langle\vec{\zeta}_i(t)\rangle = 0, \quad (6)$$

$$\left\langle\zeta_i^{\eta}(t)\zeta_j^{\theta}(t')\right\rangle = \frac{2k_B T\alpha\mu_s}{\gamma}\delta_{ij}\delta_{\eta\theta}\delta(t-t'). \quad (7)$$

Here i, j denote lattice sites, and η and θ are Cartesian components of the stochastic noise.

III. RESULTS AND DISCUSSION

A. Magnetism of θ-phase bulk MnN

First, we investigate a bulk MnN system starting from first principles. For the model we implement the geometry of the experimentally observed θ-phase of MnN, which is a NaCl structure with $a = 4.256$ Å and $c = 4.189$ Å. In Fig. 1, the isotropic exchange interactions J_{ij}^{iso} and the biquadratic couplings B_{ij} are shown as a function of the distance between the Mn atoms. According to Eq. (1), the positive and negative sign of J_{ij}^{iso} refers to FM and AF coupling, respectively. As can be inferred from Fig. 1, the isotropic couplings are dominated by strong FM second-nearest-neighbor (NN) and by considerably weaker AF first-NN interactions. Due to the tetragonal distortion, $c < a$, these interactions are split: the AF interaction between nearest neighbors in subsequent MnN planes along the c direction is stronger than that within the same plane, while this relation is opposite for the FM second-NN interactions. Similarly to the isotropic bilinear couplings, the first- and second-NN biquadratic couplings also split. Since their magnitude is smaller by at least one order compared with that for the bilinear couplings, they will not affect the ground state of the system. We note, however, that

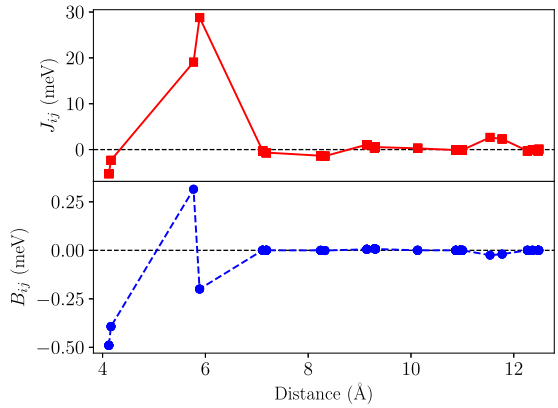

FIG. 1. Calculated isotropic exchange interaction parameters, J_{ij}^{iso}, and biquadratic couplings, B_{ij}, as a function of distance between Mn atoms.

for the MnN/Fe interface they have a strength comparable to the Dzyaloshinskii-Moriya interactions.

We also calculated the on-site and the two-site anisotropies, $K \approx -0.08$ meV and $\Delta J \approx -0.02$ meV, where the negative sign refers to an easy c-axis normal to the planes as sketched in the inset of Fig. 2. Note that the tetragonal distortion of the MnN lattice does not break the inversion symmetry; therefore, the DM interactions overall cancel each other. The spin moment of Mn, $\mu_{\mathrm{Mn}} = 2.84\mu_{\mathrm{B}}$, was obtained from the self-consistent electronic structure calculation in the DLM state.

Using the spin-model parameters in Eq. (1), we determined the magnetic ground state of bulk MnN and its magnetic properties at finite temperatures by employing the SLLG Eq. (4). We used 10 976 sites populated by classical spins with a periodic boundary condition, and we considered the full tensorial exchange interactions, the on-site anisotropy, and the biquadratic term. For the ground-state calculations, the simulations were initialized by random spin configurations

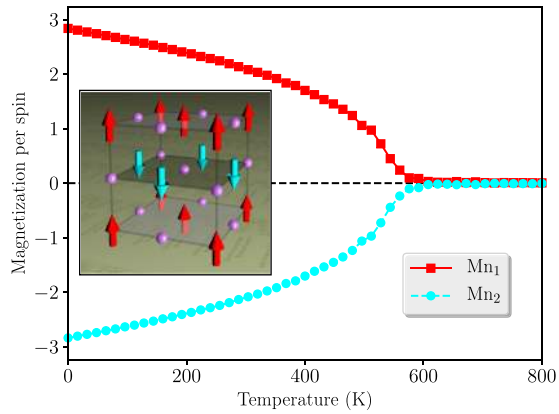

FIG. 2. Calculated magnetization curve of the two sublattices of Mn in bulk MnN as a function of the temperature. The inset illustrates the magnetic ground state of MnN. Violet spheres represent the N atoms, while red and blue arrows correspond to the spin moments of Mn_1 and Mn_2 atoms, respectively.

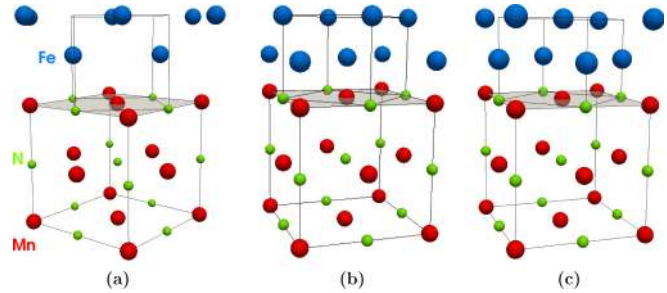

FIG. 3. Three investigated stacking structures of the Mn/Fe interface: (a) Fe above hollow position, (b) Fe above Mn, and (c) Fe above N. Fe, N, and Mn atoms are represented by blue, green, and red spheres respectively.

and continued until the normalized magnetic torque, $\frac{\vec{s}_i \times \vec{H}_i}{|\vec{H}_i|}$, became smaller than 10^{-6}.

The simulated magnetic ground state is sketched in the inset of Fig. 2. It is composed of two magnetic sublattices, Mn_1 and Mn_2, forming a layered AF state. This magnetic configuration results from the strong FM second-NN couplings and the previously mentioned lifting of the first-NN AF exchange interactions, which favors an antiparallel alignment of Mn spins in two consecutive MnN layers along the c direction. Due to the negative value of both the on-site and two-site anisotropy (see above), we find that the preferred orientation of the Mn spins is along the c axis.

Once the magnetic ground state was determined, we evaluated the thermal dependence of the bulk MnN using Langevin dynamics. In Fig. 2, the temperature dependence of the magnetization of the two sublattices of Mn are shown. As the two sublattices are identical, the same temperature dependence with opposite magnetizations is obtained. To evaluate the critical temperature, we fit the function $M_\alpha(T) = M_\alpha(0)(\frac{T_N - T}{T_N})^\beta$ to the magnetization data, where $\alpha = 1, 2$. From this fit, the obtained Néel temperature is $T_N \approx 570$ K, which is in good agreement with the experimental value of 660 K [19].

B. Spin model parameters of the MnN/Fe interface

To investigate the possibility of using MnN as an AF for exchange bias, we evaluated the interface structure of MnN/Fe. For the MnN side the experimentally known geometry is used, and on the FM side a bcc structure for Fe is assumed. Due to the close match of the corresponding in-plane lattice constants, three possible stacking arrangements of the atoms at the interface MnN/Fe layer were considered, as shown in Fig. 3. Using the *ab initio* VASP code [32–34] with a $6 \times 6 \times 1$ k-point sampling of the Brillouin zone and employing the GGA-PBE exchange functional, these three geometries were optimized. For the geometry optimization, we used a supercell consisting of 12 Mn, 12 N, and 8 Fe atoms, i.e., 6 MnN and 4 Fe layers. The atoms in the bottom three MnN layers were fixed to their bulk positions, while three MnN layers and four Fe layers at the interface were freely relaxed in the perpendicular direction. The in-plane lattice constant of the supercell was kept fixed, thus in-plane relaxation was not allowed. In each of the three stacking geometries, the total

TABLE I. Calculated total energies (in eV) relative to the energy minimum (0): $\Delta E_{\text{tot}}^{\text{FM-MnN}}$ and $\Delta E_{\text{tot}}^{\text{AF-MnN}}$ for all three considered MnN-Fe stackings and FM-MnN and AF-MnN magnetic configurations. Note that the spin moments in the Fe layer are FM coupled to those in the neighboring MnN layer.

	$\Delta E_{\text{tot}}^{\text{FM-MnN}}$	$\Delta E_{\text{tot}}^{\text{AF-MnN}}$
Fe above N	0.78	0
Fe above hollow	2.64	1.62
Fe above Mn	4.27	3.45

energies are calculated in two collinear magnetic configurations, where the spin moments in the MnN planes are coupled either FM or AF to each other, while the Fe moments are always FM coupled to those of the neighboring MnN layer at the interface. Table I reports the relative total energies of the considered geometric and magnetic configurations, where the zero value corresponds to the energetically favored one, which is the Fe-above-N geometry [see Fig. 3(c)] with AF configuration for the MnN layer.

We found that the interface layers are relaxed with -3% for the MnN and -12% for the Fe relative to the interlayer distance of the bulk MnN, where the negative sign corresponds to an inward layer relaxation. In the subsequent calculations of the magnetic properties of the MnN/Fe system, the above relaxations of the interface layers were taken into account.

Once the optimal stacking geometry at the MnN/Fe interface was determined, we self-consistently calculated the electronic and magnetic structures near the interface using the SKKR method, and we obtained the magnetic interactions from the paramagnetic phase via the spin-cluster expansion technique. The first-principles results indicate that the magnetic properties on both the MnN and the Fe sides are modified in the vicinity of the interface. This is demonstrated in Fig. 4 in terms of the layer-resolved magnetic moments and the on-site and two-site anisotropies. The atomic layers along the z direction (perpendicular to the interface) are labeled by index

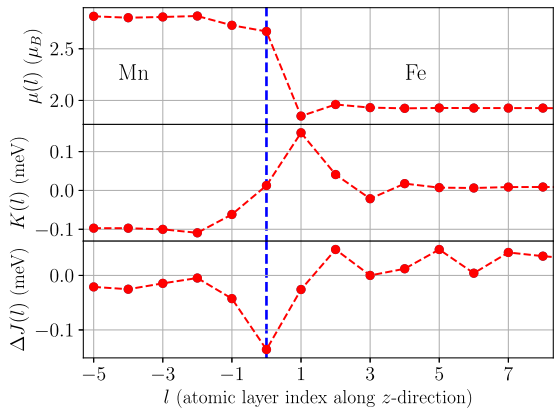

FIG. 4. Calculated layer-resolved spin magnetic moments $\mu(l)$, on-site, and two-site anisotropies, $K(l)$ and $\Delta J(l)$, as a function of the atomic layers labeled by l. Negative and positive signs of $K(l)$ and of $\Delta J(l)$ correspond to out-of-plane and in-plane preferred directions of the spin moments, respectively. The blue vertical line denotes the Mn layer at the interface.

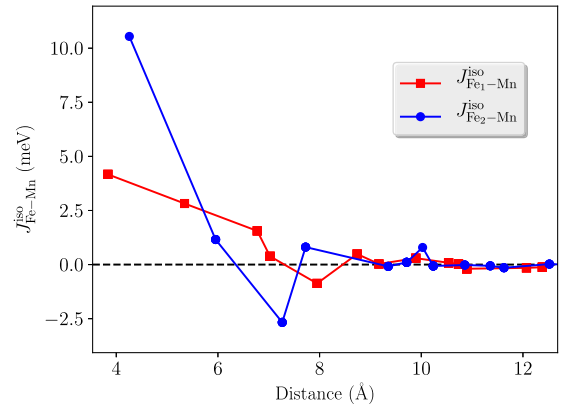

FIG. 5. Calculated isotropic exchange interactions between the Fe atoms in the first Fe layer ($l = 1$) and the Mn atoms, $J^{\text{iso}}_{\text{Fe}_1\text{-Mn}}$, and between the Fe atoms in the second Fe layer ($l = 2$) and the Mn atoms, $J^{\text{iso}}_{\text{Fe}_2\text{-Mn}}$, as a function of the distance between the Fe and Mn atoms.

l, where $l = 0$ corresponds to the interface (the last layer of the AF MnN). A reduction of the magnitude of the magnetic moment at $l = 0$ is observed, and away from the interface the Fe spin moment is nearly constant. The magnitude of the on-site anisotropy $K(l)$ at the Mn layers is clearly reduced with respect to its bulk value, and it practically vanishes at the interface Mn layer $l = 0$. The two-site anisotropy $\Delta J(l)$ in the AFM part is also strongly affected by the interface as it takes even a positive value for $l = -2$, but it becomes again slightly negative close to the interface ($l = -1$ and 0). As a consequence, the Mn spin moments keep their preference for an out-of-plane orientation at the interface. At the AF side, for farther layers from the interface ($l < -2$), $K(l)$ and $\Delta J(l)$ are saturated to around the bulk values, -0.08 and -0.02 meV, respectively. At the FM side, the Fe layers mainly exhibit a weak in-plane magnetocrystalline anisotropy as can be inferred from the sums of the corresponding on-site and two-site contributions. The spin moment of Fe is saturated at the value of $1.94\mu_B$. Note that this is smaller than the spin moment of Fe in a bulk FM state ($\sim 2.2\mu_B$). The reason is that the self-consistent calculations were performed in the paramagnetic state using DLM theory, where a softening of the Fe spin moment occurs as was reported recently [35].

It is well known that the EB effect is primarily related to the interactions between FM/AF magnetic moments, therefore in the rest of this section we focus on the magnetic interactions between the Fe and the Mn moments across the interface. In Fig. 5, the isotropic exchange interactions between Fe-Mn spin moments are shown as a function of the distance between Fe-Mn atoms for the first and the second Fe layer. We find that the Fe-Mn isotropic exchange interactions are mainly FM, and the first-shell coupling of Fe_2-Mn is the strongest.

In contrast to bulk MnN, there are remarkable DM interactions at the MnN/Fe interface as shown in Fig. 6. The first-NN DM interaction between Fe_1 and Mn is the largest, and the second-NN DM vector cancels due to the C_{4v} symmetry. Note that, for the same reason, all DM vectors are in-plane. Beyond the DM interaction between Mn and Fe atoms in $l = 1$ and 2 layers, the first-NN DM interaction between Fe_3 and Mn is

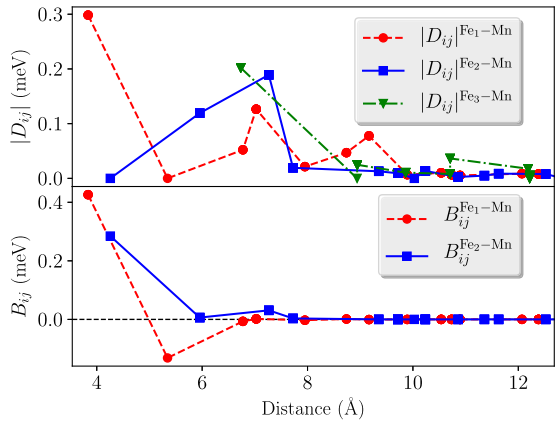

FIG. 6. Magnitude of the DM vectors $|D_{ij}|$ and biquadratic couplings B_{ij} between Fe and Mn spin moments, selecting the Fe atoms from the first ($l = 1$) and second ($l = 2$) layer from the interface as in Fig. 5. Note that $|D_{ij}|$ is also shown for the third ($l = 3$) Fe layer.

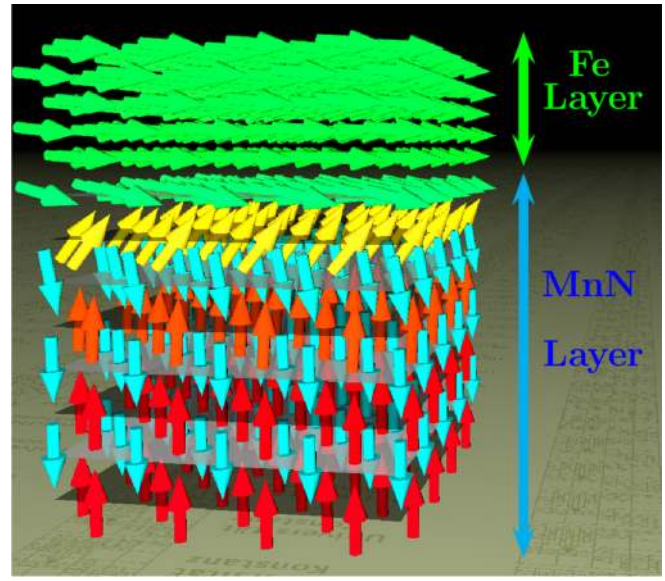

FIG. 7. Simulated magnetic state of the MnN/Fe system near the interface after the field-cooling process in an external cooling field, $H_{\mathrm{cf}} = 1$ T. The arrows illustrate the direction of the magnetic moments of Mn and Fe atoms. The green arrows in the top five atomic layers correspond to the spin components of Fe atoms. The bottom-layer green arrows and the yellow arrows directly below represent the spin moments of the Mn atoms near the interface, while red and cyan arrows correspond to the two Mn sublattices of the MnN.

still relevant, because it is larger than all the DM interactions between Fe_2 and Mn. The biquadratic couplings are also shown in Fig. 6 as a function of the distance between the Fe and Mn atoms. The Fe-Mn biquadratic couplings are mostly positive, and this, together with the dominating FM isotropic exchange interactions, would favor a parallel configuration between Fe and Mn spin moments. This, however, is in competition with magnetic anisotropies, which would favor out-of-plane orientation for bulk MnN but in-plane orientation for the Fe layer.

C. Exchange-bias effect in MnN/Fe

We simulated hysteresis loops for the MnN/Fe bilayer system by solving the stochastic Landau-Lifshitz-Gilbert (LLG) equation in the context of the generalized Heisenberg model as described in Eq. (1), where the exchange interactions are considered up to 11th NNs (distance cutoff $d_{\mathrm{Co}} = 2.01a_{\mathrm{2D}}$). Prior to calculating the hysteresis loops, we prepared the system similar to experiments by simulating a field-cooling (FC) process. The FC process starts from a random spin configuration in the AF part, at an initial temperature T above the Néel temperature of the AF but below the Curie temperature of the FM, and proceeds to a final temperature $T_f = 0$ K under the influence of an external applied (cooling) field, $H_{\mathrm{cf}} = 1$ T.

Figure 7 shows the resulting spin configuration of a MnN/Fe interface consisting of five atomic layers of Fe and eight Mn sublattices. The Fe moments are oriented in the interface plane, following the external field. The orientation of the Mn spins away from the interface is mainly along the z direction, perpendicular to the interface. Close to the interface, however, the spin moments in the Mn layers are tilted away from the out-of plane direction, while in the case of $l = 0$ the Mn moments are mainly oriented in-plane and present a net magnetization parallel to the Fe moments. Here, their orientation results from the strong ferromagnetic exchange interactions for the first and second shells between the Fe and Mn atoms (see Fig. 5), which favors a parallel orientation of the NN Fe-Mn atoms in-plane. The bi-quadratic coupling between Fe-Mn atoms at the interface also favors a parallel orientation between the Fe-Mn moments (see Fig. 6). Moreover, the on-site anisotropies for the interface Mn layer and Fe layers favor an in-plane orientation of the Fe and Mn moments (see Fig. 4).

While simulating hysteresis loops, the applied field axis is along the cooling field direction. During the switching process, the Fe moments rotate coherently in-plane. We also observe that during this rotation, the tilted Mn moments at the interface follow the Fe magnetization, due to the ferromagnetic character of the Fe-Mn interface exchange interactions. But this net magnetization of the AF is not purely contained in the plane: rather, because of a lack of compensation at the interface, a net magnetic moment of $\mu(\mathrm{AF}) \approx -0.11\mu_B$ in the z-direction arises, which remains nearly constant during the hysteresis loop.

1. Variation of the AF thickness

We simulated the hysteresis loops of the MnN/Fe bilayer for several values of the AF thickness, t_{AF}, and we analyze the influence of the AF thickness on the coercive and exchange-bias fields. The EB field is numerically evaluated as

$$H_{\mathrm{EB}} = -\frac{H_c^+ + H_c^-}{2}, \tag{8}$$

where $H_c^{+,-}$ denote the coercive fields during the descending ($-$) and ascending ($+$) branch of the hysteresis loops. The

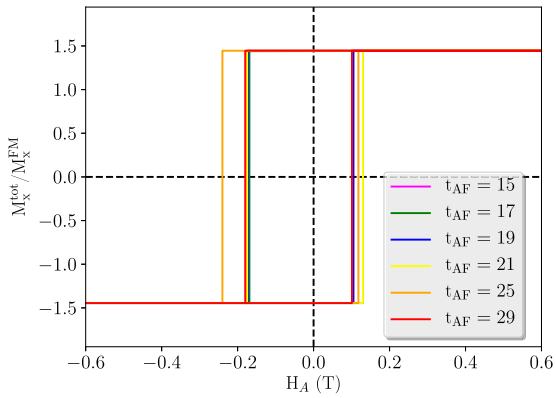

FIG. 8. Calculated in-plane hysteresis loops as a function of the AF thickness, t_{AF} (in ML), for $t_{FM} = 5$ ML. Here, M_x^{tot} and M_x^{FM} denote the x magnetization component of the total system and the ferromagnetic side, respectively.

overall coercive field is then

$$H_C = \frac{H_c^+ - H_c^-}{2}, \tag{9}$$

In Fig. 8, in-plane hysteresis loops for MnN/Fe bilayers with fixed FM layer thickness, $t_{FM} = 5$ ML, are shown for several thicknesses of the AFM layer. These hysteresis loops are clearly rectangular due to the coherent rotation of the ferromagnet, with constant remanent magnetization for the different AF thicknesses. The value of the coercive field varies slightly with a minimum of approximately 140 mT for $t_{AF} = 17$ ML and a maximum of approximately 180 mT for $t_{AF} \approx 25$ ML (see Fig. 9).

Furthermore, we observe an in-plane EB effect, characterized by the horizontal shift of the hysteresis loops. The obtained EB fields as a function of the AF thickness are also shown in Fig. 9. The EB field varies nonmonotonically as a function of the AF thickness, but there is an overall tendency for larger EB fields with increasing AF film thickness. These results are in agreement with the experimental results reported for the case of MnN/CoFe bilayers, where the EB field also increases with the AF thickness until reaching a maximum of about 180 mT for an AF film thickness of about 30 nm [17].

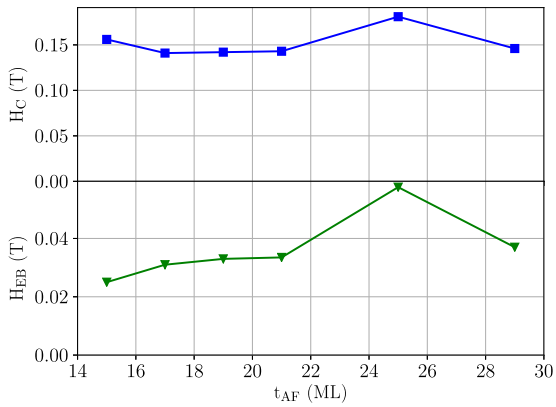

FIG. 9. Calculated coercive, H_C, and exchange-bias fields, H_{EB}, as a function of the AF thickness, t_{AF}.

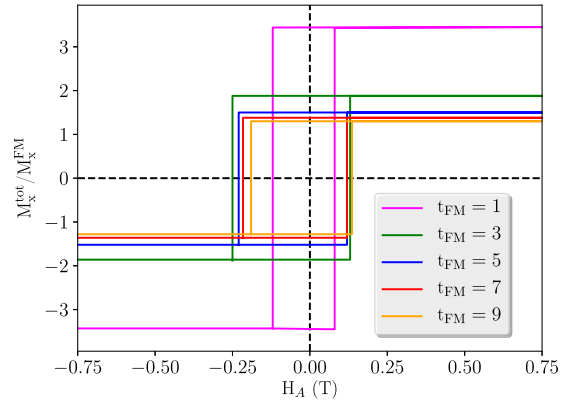

FIG. 10. Calculated in-plane hysteresis loops as a function of the FM thickness, t_{FM} (in ML), in the case of $t_{AF} = 25$ ML. Here, M_x^{tot} and M_x^{FM} denote the x magnetization component of the total system and the ferromagnetic side, respectively.

Note that in our simulations, the MnN thicknesses are below the experimental values.

The origin of the EB effect can be deduced from the spin structure shown in Fig. 7. Since the Dzyaloshinskii-Moriya interaction at the interface is chiral, the spin configuration shown here is energetically not equal to the corresponding state with reversed magnetization of the FM. This is even true when we assume that the tilted spins in the AF (mostly the yellow spins) follow the FM and are finally tilted toward the new, reversed direction of the spin of the FM. This symmetry is broken by the Dzyaloshinskii-Moriya interaction, leading to an energetic difference of the two states and, with that, to EB.

2. *Variation of the FM thickness*

Next, we investigated the dependence of the coercive and EB fields on the thickness of the FM, t_{FM}. Figure 10 shows the calculated hysteresis loop of our MnN/Fe system as a function of the FM thickness for a fixed thickness of the AF layer of $t_{AF} = 25$ ML. Again, the reversal mechanism is a coherent rotation, and the shapes of the hysteresis curves are rectangular. In contrast to the case of the variation of t_{AF}, the remanent magnetization is not constant. This is due to the fact that the AFM also contributes to the total magnetization, because of the tilting of the AF spins at the interface, shown in Fig. 7. Since we normalize to the magnetic moment of the FM, the normalized saturation values are always above unity, converging to 1 for large thickness of the FM (see also Fig. 11).

The coupling between the FM and the AF is solely via the interface, and consequently one expects a decreasing influence of the AF with increasing thickness of the FM layer [36]. This behavior was observed experimentally [17], and in Fig. 11 we also find for both the coercive and EB fields a decrease with increasing FM thickness for thicknesses above $t_{FM} = 3$ ML. For thinner FM layers, the interactions across the interface cannot be considered constant since the Fe-Mn interactions go clearly beyond nearest neighbors and build up with the number of FM monolayers until a saturation is reached (see Fig. 5).

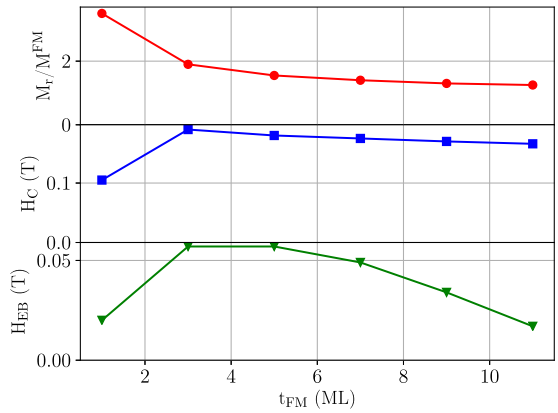

FIG. 11. Calculated relative remanence magnetization, coercive, H_C, and exchange-bias fields, H_{EB}, as a function of the FM thickness, t_{FM}, in the case of $t_{AF} = 25$ ML.

IV. CONCLUSION

Combining *ab initio* and spin-dynamics simulations, we investigated the magnetic properties of bulk MnN and at a MnN/Fe interface. First, we determined the tensorial exchange interactions and biquadratic couplings between Mn atoms for the θ-phase of bulk MnN. We found that the first-NN isotropic exchange interactions are antiferromagnetic while the second-NN interactions are strongly ferromagnetic, and the interplay of these interactions results in an AF-I type magnetic ground state. Using these spin-model parameters, we obtained the Néel temperature of bulk MnN in good agreement with experiment. For the MnN/Fe interface, the spin-model parameters were determined based on previously optimized geometry. We found that near the interface, the spin moments of the Mn and Fe atoms are ferromagnetically coupled and they prefer a direction parallel to the plane of the interface. Since the spins of the Mn atoms are oriented out-of-plane when moving farther away from the interface, a twisted spin structure is formed across the interface. Hysteresis loops of the MnN/Fe bilayer were evaluated after a field-cooling process, and a large exchange-bias effect was found due to sizable Dzyaloshinskii-Moriya interactions across the MnN/Fe interface. The variations of the exchange-bias effect as a function of the thickness of the FM and AF layers were also investigated. We found that the coercive and exchange-bias fields have maximal values at around 25 ML AF thickness, and these field values are decreasing with increasing FM thickness.

ACKNOWLEDGMENTS

This work was supported by the European Commission via the Collaborative Project HARFIR (Project No. 604398), by the National Research, Development and Innovation Office of Hungary under Projects No. K115575, No. PD120917, and No. FK124100, by the Slovak Academy of Sciences SASPRO Project No. 1239/02/01, and by the BME-Nanotechnology FIKP grant of EMMI (BME FIKP-NAT). We also acknowledge NIIF for providing access to the resource based in Hungary at Debrecen.

[1] W. H. Meiklejohn and C. P. Bean, Phys. Rev. **102**, 1413 (1956).
[2] A. P. Malozemoff, Phys. Rev. B **35**, 3679 (1987).
[3] W. Kuch, L. I. Chelaru, F. Offi, J. Wang, M. Kotsugi, and J. Kirschner, Nat. Mater. **5**, 128 (2006).
[4] P. Miltényi, M. Gierlings, J. Keller, B. Beschoten, G. Güntherodt, U. Nowak, and K. D. Usadel, Phys. Rev. Lett. **84**, 4224 (2000).
[5] U. Nowak, K. D. Usadel, J. Keller, P. Miltényi, B. Beschoten, and G. Güntherodt, Phys. Rev. B **66**, 014430 (2002).
[6] I. K. Schuller, R. Morales, X. Batlle, U. Nowak, and G. Güntherodt, J. Magn. Magn. Mater. **416**, 2 (2016).
[7] F. Nolting, A. Scholl, J. Stöhr, J. W. Seo, J. Fompeyrine, H. Siegwart, J. P. Locquet, S. Anders, J. Lüning, E. E. Fullerton, M. F. Toney, M. R. Scheinfein, and H. A. Padmore, Nature (London) **405**, 767 (2000).
[8] D. Lederman, R. Ramírez, and M. Kiwi, Phys. Rev. B **70**, 184422 (2004).
[9] G. Vallejo-Fernandez, L. E. Fernandez-Outon, and K. O'Grady, J. Phys. D **41**, 112001 (2008).
[10] Y. Ijiri, T. C. Schulthess, J. A. Borchers, P. J. van der Zaag, and R. W. Erwin, Phys. Rev. Lett. **99**, 147201 (2007).
[11] S. Dong, K. Yamauchi, S. Yunoki, R. Yu, S. Liang, A. Moreo, J.-M. Liu, S. Picozzi, and E. Dagotto, Phys. Rev. Lett. **103**, 127201 (2009).
[12] R. Yanes, J. Jackson, L. Udvardi, L. Szunyogh, and U. Nowak, Phys. Rev. Lett. **111**, 217202 (2013).
[13] M. Ali, C. H. Marrows, M. Al-Jawad, B. J. Hickey, A. Misra, U. Nowak, and K. D. Usadel, Phys. Rev. B **68**, 214420 (2003).
[14] J. P. Nozières, S. Jaren, Y. B. Zhang, A. Zeltser, K. Pentek, and V. S. Speriosu, J. Appl. Phys. **87**, 3920 (2000).
[15] M. Rickart, A. Guedes, J. Ventura, J. B. Sousa, and P. P. Freitas, J. Appl. Phys. **97**, 10K110 (2005).
[16] A. Hirohata, T. Huminiuc, J. Sinclair, H. Wu, M. Samiepour, G. Vallejo-Fernandez, K. O'Grady, J. Balluf, M. Meinert, G. Reiss, E. Simon, S. Khmelevskyi, L. Szunyogh, R. Y. Díaz, U. Nowak, T. Tsuchiya, T. Sugiyama, T. Kubota, K. Takanashi, N. Inami, and K. Ono, J. Phys. D **50**, 443001 (2017).
[17] M. Meinert, B. Büker, D. Graulich, and M. Dunz, Phys. Rev. B **92**, 144408 (2015).
[18] W. R. L. Lambrecht, M. Prikhodko, and M. S. Miao, Phys. Rev. B **68**, 174411 (2003).
[19] A. Leineweber, R. Niewa, H. Jacobs, and W. Kockelmann, J. Mater. Chem. **10**, 2827 (2000).
[20] K. Suzuki, Y. Yamaguchi, T. Kaneko, H. Yoshida, Y. Obi, H. Fujimori, and H. Morita, J. Phys. Soc. Jpn. **70**, 1084 (2001).
[21] M. S. Miao and W. R. L. Lambrecht, Phys. Rev. B **71**, 214405 (2005).
[22] L. Szunyogh, B. Újfalussy, P. Weinberger, and J. Kollár, Phys. Rev. B **49**, 2721 (1994).
[23] R. Zeller, P. H. Dederichs, B. Újfalussy, L. Szunyogh, and P. Weinberger, Phys. Rev. B **52**, 8807 (1995).
[24] B. L. Gyorffy, A. J. Pindor, J. Staunton, G. M. Stocks, and H. Winter, J. Phys. F **15**, 1337 (1985).

[25] L. Szunyogh, L. Udvardi, J. Jackson, U. Nowak, and R. Chantrell, Phys. Rev. B **83**, 024401 (2011).
[26] L. Udvardi, L. Szunyogh, K. Palotás, and P. Weinberger, Phys. Rev. B **68**, 104436 (2003).
[27] I. Dzyaloshinsky, J. Phys. Chem. Solids **4**, 241 (1958).
[28] T. Moriya, Phys. Rev. Lett. **4**, 228 (1960).
[29] A. Lyberatos, D. V. Berkov, and R. W. Chantrell, J. Phys.: Condens. Matter **5**, 8911 (1993).
[30] U. Nowak, Classical spin models, in *Handbook of Magnetism and Advanced Magnetic Materials* (Wiley, Chichester, 2007).
[31] J. L. García-Palacios and F. J. Lázaro, Phys. Rev. B **58**, 14937 (1998).
[32] G. Kresse and J. Furthmüller, Comput. Mater. Sci. **6**, 15 (1996).
[33] G. Kresse and J. Furthmüller, Phys. Rev. B **54**, 11169 (1996).
[34] J. Hafner, J. Comput. Chem. **29**, 2044 (2008).
[35] A. Deák, E. Simon, L. Balogh, L. Szunyogh, M. dos Santos Dias, and J. B. Staunton, Phys. Rev. B **89**, 224401 (2014).
[36] J. Nogués and I. K. Schuller, J. Magn. Magn. Mater. **192**, 203 (1999).